Chemical Science

EDGE ARTICLE

View Article Online
View Journal | View Issue

Cite this: *Chem. Sci.*, 2015, **6**, 3572

Edge overgrowth of spiral bimetallic hydroxides ultrathin-nanosheets for water oxidation†

Bing Ni and Xun Wang*

Received 7th March 2015
Accepted 2nd April 2015

DOI: 10.1039/c5sc00836k

www.rsc.org/chemicalscience

The structure of edges may dramatically influence the properties of nanomaterials, so the rational design or control over the structures of the edges is required. Here we synthesized spiral ultrathin-nanosheets with overgrown edges (SUNOE) of NiFe, CoNi and CoFe bimetallic hydroxides by governing the growth rates of different directions in screw dislocation driven growth (SDDG) in nonaqueous solvents. The driving force for the SDDG is supersaturation, which could be controlled by the concentration of the different precursors, thus achieving non-uniform structures of the edges and inner sheets. NiFe, CoNi and CoFe bimetallic hydroxides possess layered structures, in which overgrown edges may prevent them from re-stacking. The as prepared SUNOE all show good performance for the oxygen evolution reaction (OER) in the electrolysis of water, and the lowest onset potential was 1.45 V (*vs.* RHE) (the lowest potential when the current density reached 10 mA cm^{-2} was 1.51 V (*vs.* RHE)).

Introduction

Usually the edges of nanomaterials show unique properties different to the faces. For example, one of the central problems in the field of graphene-related research is how it behaves with different edge structures.[1–3] In transition-metal dichalcogenides (TMDs) the properties of atoms on the edges are different to atoms on the basal planes.[4–7] While increasing the content of atoms at the edges of noble metal nanoparticles can greatly enhance the catalytic properties.[8] To some extent, well-designed edges can give a promising future for the applications of nanomaterials. Spiral TMDs have been achieved in recent studies,[9,10] however, their edge structures are less studied. Spiral structures are usually achieved *via* screw dislocation driven growth (SDDG). The driving force for SDDG is supersaturation, which can be controlled by the concentration of different precursors, thus achieving non-uniform structures of edges and inner sheets.

In most cases, the edges of nanostructures are just the natural ends of the faces of the particles. Etching is a probable method to tune the environment around edges,[11–13] this can be seen as a "top-down" method. However, it is always important to figure out diverse solutions for certain goals and identify many more possibilities. Herein we present a "bottom-up" solution to design the edges of nanosheets, by the SDDG of crystals. SDDG is a classic example to illustrate crystal growth in low supersaturation.[14,15] The crystal grows from a screw dislocation and enlarges with two competitive rates, one is an in-plane rate, r_i, and the other is a vertical rate, r_v.[16–19] We controlled these two rates by the concentrations of the precursors in a non-aqueous solvent, and thus achieved the overgrowth of edges in ultrathin-nanosheets. The final morphologies are spiral ultrathin nanosheets with overgrown edges (SUNOE) (Fig. 1 and 2). The discernible spokewise edges indicate a SDDG mechanism. Edge overgrowth has shown strength in the synthesis of nanoparticles enclosed by high index facets.[20,21] Such a strategy requires a judicious control over the precursors and surface chemistry. Herein the edge overgrowth driven by the change in the concentrations during the SDDG provides another easily accessible and highly controllable method to fabricate novel structures. As a proof of concept, the report here illustrates the feasibility to prepare edge overgrowth in two dimensional materials.

The alpha phase of the metal hydroxide species can possess layered structures similar to layered double hydroxides.[22,23] We chose them as the studied materials, not only because the rules studied here may extend to other cutting-edge research in layered structures, such as graphene and TMDs, but also because of the inherent difference between the *a*–*b* direction and the *c* direction, which meant that we could utilize the different growth rates in the *a*–*b* plane and vertical to the *a*–*b* plane. Meanwhile, earth abundant hydroxides, like NiFe layered double hydroxides, are effective catalysts for the OER.[24,25] Water splitting is a hot topic for energy conversion and conservation.[26] For the electrolysis of water, the anodic overpotential is the main obstacle.[27] Therefore, investigating catalysts with a low overpotential for the OER is both meaningful and valuable.

Department of Chemistry, Tsinghua University, Beijing, 100084, China. E-mail: wangxun@mail.tsinghua.edu.cn

† Electronic supplementary information (ESI) available. See DOI: 10.1039/c5sc00836k

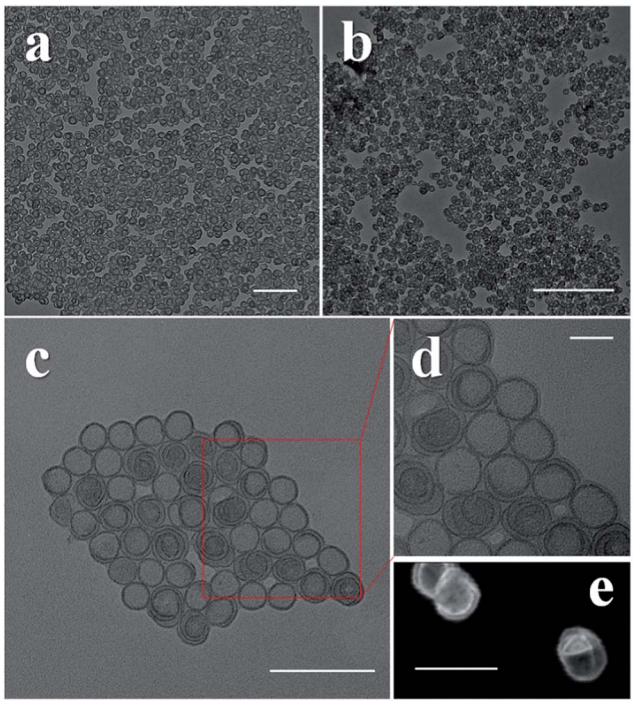

Fig. 1 TEM images of CoNi (a), CoFe (b) and NiFe (c and d) SUNOE, the color of the edges is darker than that of the inner sheets; (e) STEM image of NiFe showing ultrathin spiral sheets structures, the ultrathin sheets could be folded. Scale bar: (a) 200 nm; (b) 500 nm; (c) 100 nm; (d) 20 nm; (e) 50 nm.

Results and discussion

In a typical synthesis, two metal salts were required, one was a sulfate and the other was a chloride, the ratio was optimized for the different products. For all the salts containing water in their lattice, we avoided adding extra water into the system. After the salts were weighed and transferred into an autoclave, ethanol and either oleylamine or octaylamine were injected. After sonication and the addition of hexane, the autoclave was sealed and put into an oven which was set at specific temperature and time (details in ESI†). X-ray diffraction (XRD) data, X-ray photoelectron spectroscopy (XPS) and Fourier transform infrared spectroscopy (FT-IR spectroscopy) data suggest alpha phase structures of NiFe, CoNi and CoFe hydroxides with SO_4^{2-} intercalation (Fig. S1–S3†).

As we can see in the transmission electron microscopy (TEM) images, the final products were pure SUNOE (Fig. 1 and S4†). The details of the various SUNOE were studied at a higher magnification (Fig. 1d and 2a–c) and with high angle annular dark field scanning transmission electron microscopy (HAADF-STEM) (Fig. 1e and 2d, f, g). The sheet diameters for these three kinds of SUNOE were about 30–50 nm, and the dark edges in the TEM image were about 1 nm. For the NiFe SUNOE, there are two kinds of sheets with overgrown edges, one is a single layer sheet and the other is a spiral sheet. Single layer sheets may be formed due to the lack of a screw dislocation or a re-linking of the staggered edges of the spiral sheets. The edges of the CoFe SUNOE are more likely to be in concentric circles, like growth rings in a tree. From the STEM (Fig. 2d, f and g) and the high resolution scanning electron microscopy (HRSEM) images (Fig. 2e), we can clearly see a spiral structure and that some of the sheets are broken or folded because of the ultrathin inherence. By taking account of all the aforementioned data, we can be assured that the products are layered spiral nanosheets with overgrown edges, and that the SUNOE grew in a screw dislocation driven way.

From the TEM and STEM images, we can easily see that the contrasts of the edges and the inner sheets are different. Could there then be a difference in their chemical components? By using the energy dispersive spectroscopy line scan, we further investigated the differences between the edges and the inner sheets. For each kind of product, more than 10 single SUNOE were tested to get solid results, and all of them were highly consistent (Fig. 2g and S5†). For all such SUNOE, the ratio of the metal to S (SO_4^{2-} by FT-IR) varies from the inner sheets to the edges, showing a much higher value for the edges. The amount of S decreases at the edges, while the amount of metal shows a sudden increase at the edges. The peaks are broadened due to the drift of samples during the tests. The results are the same in all three products, suggesting that the edges are suddenly enriched as hydroxides while the inner sheets keep growing as SDDG, showing an inherent growth mechanism of such SUNOE. The driving force for this transition may be the concentration of SO_4^{2-}. Fig. S6† shows the products under different amounts of SO_4^{2-}, the SUNOE could only be obtained under an optimized concentration.

The growth of the SUNOE followed the mechanism shown in Fig. 3. The hydroxides are formed *via* the dehydration of the dissolved precursors. In these nonaqueous conditions, the solvent molecules will not interfere with the dehydration process of the precursors, thus the reaction can happen in relatively mild conditions compared with those in an aqueous solvent. Previous research has shown that ultrathin hydroxides can be obtained by the exfoliation of bulk hydroxides with the help of the intercalation of various anions.[28,29] In this "bottom-up" case, SO_4^{2-} could inhibit the stack of layers in a crystallographic way. In other words, the growth rate vertical to plane is dramatically hindered, thus the sheets are limited in the vertical direction and form an ultrathin structure. Meanwhile heteroatoms can help to form the screw dislocations.[19] Hetero metal ions are also important for forming screw dislocations, altering the metal ratio would therefore help to form uniform products (Fig. S7†). The screw dislocation can break the flat structure, and make the sheets stagger like spiral stairs. In most cases of material synthesis through SDDG, the concentration of the precursors should be kept the same to ensure that the growth simply follows SDDG during the whole reaction,[16,30] thus forming uniform and large enough particles. However, the edges will grow ordinarily with such a method. The growth can be governed by the competitive r_i and r_v rates, and these two rates will determine the final morphology. Herein, SO_4^{2-} inhibits both rates but more strongly affects r_v. A larger r_v will lead to more layers in the final products, while a lower ratio of r_v to r_i will lead to a morphology of concentric circles, like in the

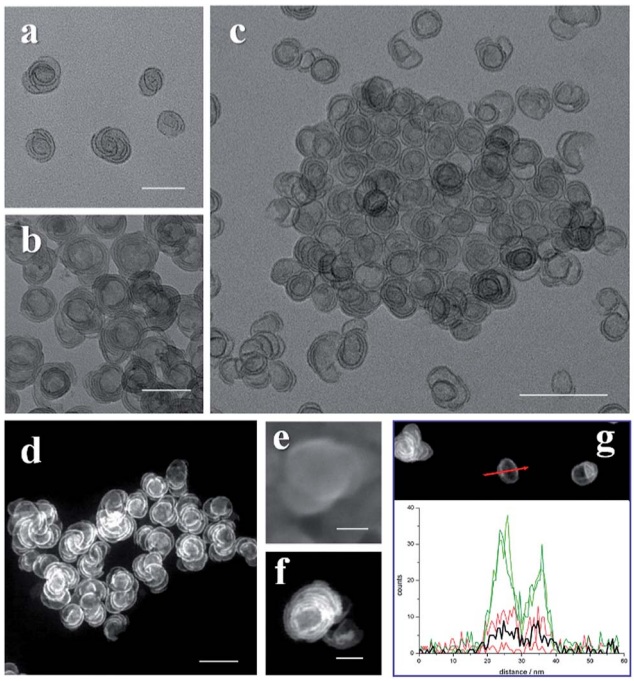

Fig. 2 TEM images of the SUNOE. The NiFe (a), CoFe (b) and CoNi (c) SUNOE products with high purities; STEM image of NiFe (g), CoFe (f) and CoNi (d) SUNOE and a HRSEM image of the CoFe (e) SUNOE clearly showing the spiral structures with overgrown edges; energy dispersive spectroscopy line scan of NiFe SUNOE (g) suggesting composition difference in edges and inner sheets, in which the red arrow shows the scan direction; the green line is used for Ni–K, the olive line for Ni–L, the red line for Fe–K, the pink line for Fe–L and the black line for S; the two peaks indicate a higher metal content in the edges. Scale bar: (a, b and d) 50 nm; (c) 200 nm; (e and f) 20 nm.

CoFe SUNOE case. After the amount of the SO_4^{2-} in the reaction medium decreases to a critical level, r_v is released and can cause overgrowth at the growth sites, resulting in the overgrowth of the edges. While, at this time, the precursors will have already been primarily used, the sudden reaction here will lead to fast consumption of all precursors and terminate the enlargement. The roles of the other parameters were also investigated (Fig. S8–S10†), the solvent composition is as important as the SO_4^{2-} concentration, since the solvent composition will influence the supersaturation of the system, which is the driving force of the SDDG. The requirements of such a method are simple and only need hetero ions to form screw dislocations and dissipative compounds to control the two growth rates, thus the method could be further extended to other systems with the consideration of the practical parameters.

The as prepared SUNOE mixed with carbon (Vulcan XC72) all show good performances for the OER. Linear sweep voltammetry (LSV) was applied to test the onset potential (Fig. 4a, all data are without iR compensation). For the pure SUNOE, the performances were ordinary with the onset potentials ranging from 1.55 V to 1.61 V. However, when carbon was added to increase the conductivity of the SUNOE, the onset potential showed a huge drop of between 50 mV to 120 mV. The best material here is the CoFe SUNOE with carbon, which showed an onset potential

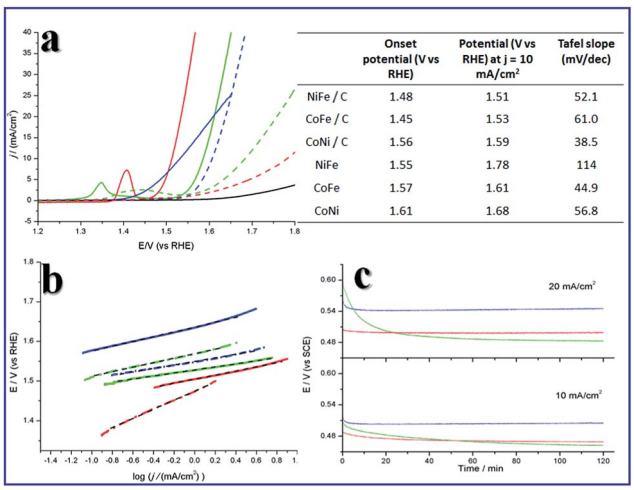

	Onset potential (V vs RHE)	Potential (V vs RHE) at j = 10 mA/cm²	Tafel slope (mV/dec)
NiFe / C	1.48	1.51	52.1
CoFe / C	1.45	1.53	61.0
CoNi / C	1.56	1.59	38.5
NiFe	1.55	1.78	114
CoFe	1.57	1.61	44.9
CoNi	1.61	1.68	56.8

Fig. 4 The OER properties of the as prepared SUNOE. The red line is used for NiFe, the blue line for CoFe and the green line for CoNi, the black line is for pure carbon (Vulcan XC72). The left of (a) is a LSV plot for each sample, solid lines are products mixed with carbon, dashed lines are used for samples without carbon. Tafel plots are shown in (b), solid line are used for products with carbon, dashed and dotted lines for samples without carbon, black dashed lines are the fitting results. Chronopotential tests at 10 mA cm^{-2} (c, lower) and 20 mA cm^{-2} (c, upper) show a decrease of potential.

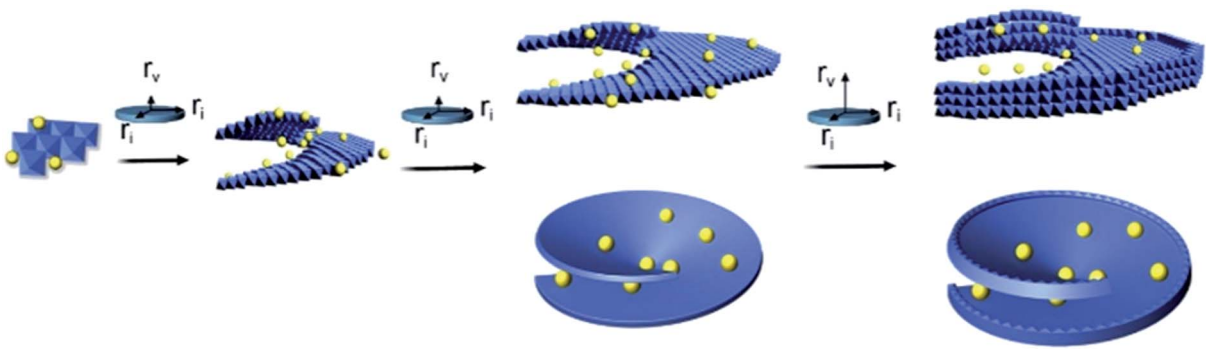

Fig. 3 Proposed growth mechanism of the SUNOE. At the beginning of the reaction, SO_4^{2-} and a hetero-cation induce the formation of a screw dislocation, the SO_4^{2-} inhibits r_v dramatically, and thus the sheets mainly enlarge in-plane, resulting in ultrathin sheets. When the concentration of SO_4^{2-} decreases to a critical level, r_v is released and causes the growth vertical to the plane.

of 1.45 V, better than the reported amorphous cobalt iron oxides.[31] The electrochemical surface area and the conductivity are two main factors which can increase the performances of catalysts.[29] The diameters of the as prepared SUNOE are about 30–50 nm, it is reasonable to consider that electrons are difficult to conduct between the different SUNOE, while the introduction of carbon can enhance the conductivity as well as the activity of the SUNOE (Fig. S12†). Meanwhile pure carbon did not show activity for the OER. The potential at $j = 10$ mA cm^{-2} is another important indicator for the real use of solar energy and water splitting.[32] Here the SUNOE mixed with carbon showed a potential down to 1.51 V, owed to the NiFe SUNOE, comparable with the recently published efficient performances.[33–35] The smallest Tafel slope here is 38.5 mV dec^{-1}, corresponding to the CoNi SUNOE. Chronopotential tests, with the current density set at 10 and 20 mA cm^{-2}, were applied to evaluate the stabilities of the as prepared materials (Fig. 4c). The potential did not increase, but, the opposite, decreased, especially for CoNi SUNOE. The effect of the anode treatment has been well studied by some groups,[36,37] and they have suggested that, after anode treatment, there would be more Co^{IV} species (Fig. S13 and S14†), and that Co^{IV}–O is beneficial for the OER. We also examined the super capacitor performance of the SUNOE (Fig. S15†), obvious bubbles were produced at the surface of the electrode while the potentials were still low. By calculating the charge stored before bubbling, we found that less than 25% of cations were oxidized. The β-$Co(OH)_2$ ultrathin-nanosheets showed a much higher specific capacitance than the layered $Co(OH)_2$ for super capacitor applications[38] and surface segregation can stabilize Ru–Ir oxides with a high OER activity.[39] This suggested to us that the overgrown edges may increase and stabilize the OER activities of the SUNOE by preventing the restacking of the ultrathin-nanosheets.

Conclusions

In conclusion, by governing the rates in the plane and vertical to plane of SDDG through the natural consumption of the precursors, the edges of the nanosheets were successfully designed to overgrow. Thus sophisticated spiral sheet structures with overgrown edges were generated, and the products showed good OER performances. It is always important to carefully design the microstructure to achieve a certain target, the growth mechanism here may be extended to synthesize other materials. Folded single layer graphene shows special band gap,[40] thus we can foresee this kind of structure in graphene or for TMDs to adopt new band gaps and new properties. The basic rules of nanocrystal formation are still in their infancy, and different rules may lead to different morphologies or structures. The use of these basic rules may open new routes for material design.

Acknowledgements

This work was supported by the NSFC (21431003, 91127040, 21221062), and the State Key Project of Fundamental Research for Nanoscience and Nanotechnology (2011CB932402).

Notes and references

1 C. Tao, L. Jiao, O. V. Yazyev, Y.-C. Chen, J. Feng, X. Zhang, R. B. Capaz, J. M. Tour, A. Zettl, S. G. Louie, H. Dai and M. F. Crommie, *Nat. Phys.*, 2011, **7**, 616–620.
2 K. Nakada and M. Fujita, *Phys. Rev. B: Condens. Matter Mater. Phys.*, 1996, **54**, 17954–17961.
3 X. Wang, Y. Ouyang, L. Jiao, H. Wang, L. Xie, J. Wu, J. Guo and H. Dai, *Nat. Nanotechnol.*, 2011, **6**, 563–567.
4 G. Xu, J. Wang, B. Yan and X.-L. Qi, *Phys. Rev. B: Condens. Matter Mater. Phys.*, 2014, **90**, 100505.
5 X. Yin, Z. Ye, D. A. Chenet, Y. Ye, K. O'Brien, J. C. Hone and X. Zhang, *Science*, 2014, **344**, 488–490.
6 T. F. Jaramillo, K. P. Jørgensen, J. Bonde, J. H. Nielsen, S. Horch and I. Chorkendorff, *Science*, 2007, **317**, 100–102.
7 H. I. Karunadasa, E. Montalvo, Y. Sun, M. Majda, J. R. Long and C. J. Chang, *Science*, 2012, **335**, 698–702.
8 W. Zhu, Y. J. Zhang, H. Zhang, H. Lv, Q. Li, R. Michalsky, A. A. Peterson and S. Sun, *J. Am. Chem. Soc.*, 2014, **136**, 16132–16135.
9 L. Zhang, K. Liu, A. B. Wong, J. Kim, X. Hong, C. Liu, T. Cao, S. G. Louie, F. Wang and P. Yang, *Nano Lett.*, 2014, **14**, 6418–6423.
10 L. Chen, B. Liu, A. N. Abbas, Y. Ma, X. Fang, Y. Liu and C. Zhou, *ACS Nano*, 2014, **8**, 11543–11551.
11 C. Chen, Y. Kang, Z. Huo, Z. Zhu, W. Huang, H. L. Xin, J. D. Snyder, D. Li, J. A. Herron, M. Mavrikakis, M. Chi, K. L. More, Y. Li, N. M. Markovic, G. A. Somorjai, P. Yang and V. R. Stamenkovic, *Science*, 2014, **343**, 1339–1343.
12 Y. Wu, D. Wang, Z. Niu, P. Chen, G. Zhou and Y. Li, *Angew. Chem., Int. Ed.*, 2012, **51**, 12524–12528.
13 J. E. Macdonald, M. Bar Sadan, L. Houben, I. Popov and U. Banin, *Nat. Mater.*, 2010, **9**, 810–815.
14 P. Smereka, *Phys. D*, 2000, **138**, 282–301.
15 Y.-I. Kwon, B. Dai and J. J. Derby, *Prog. Cryst. Growth Charact. Mater.*, 2007, **53**, 167–206.
16 F. Meng, S. A. Morin, A. Forticaux and S. Jin, *Acc. Chem. Res.*, 2013, **46**, 1616–1626.
17 S. A. Morin, A. Forticaux, M. J. Bierman and S. Jin, *Nano Lett.*, 2011, **11**, 4449–4455.
18 A. Zhuang, J. J. Li, Y. C. Wang, X. Wen, Y. Lin, B. Xiang, X. Wang and J. Zeng, *Angew. Chem., Int. Ed.*, 2014, **53**, 6425–6429.
19 T. P. Schulze and R. V. Kohn, *Phys. D*, 1999, **132**, 520–542.
20 B. Y. Xia, H. B. Wu, X. Wang and X. W. Lou, *Angew. Chem.*, 2013, **125**, 12563–12566.
21 B. Y. Xia, Y. Yan, X. Wang and X. W. Lou, *Mater. Horiz.*, 2014, **1**, 379–399.
22 R. Ma, Z. Liu, K. Takada, K. Fukuda, Y. Ebina, Y. Bando and T. Sasaki, *Inorg. Chem.*, 2006, **45**, 3964–3969.
23 J. R. Neilson, J. A. Kurzman, R. Seshadri and D. E. Morse, *Chem.–Eur. J.*, 2010, **16**, 9998–10006.
24 R. Subbaraman, D. Tripkovic, K.-C. Chang, D. Strmcnik, A. P. Paulikas, P. Hirunsit, M. Chan, J. Greeley, V. Stamenkovic and N. M. Markovic, *Nat. Mater.*, 2012, **11**, 550–557.

25 M. Gao, W. Sheng, Z. Zhuang, Q. Fang, S. Gu, J. Jiang and Y. Yan, *J. Am. Chem. Soc.*, 2014, **136**, 7077–7084.
26 A. J. Bard, *J. Am. Chem. Soc.*, 2010, **132**, 7559–7567.
27 M. W. Louie and A. T. Bell, *J. Am. Chem. Soc.*, 2013, **135**, 12329–12337.
28 Q. Wang and D. O'Hare, *Chem. Rev.*, 2012, **112**, 4124–4155.
29 F. Song and X. Hu, *Nat. Commun.*, 2014, **5**, 4477.
30 M. J. Bierman, Y. K. Lau, A. V. Kvit, A. L. Schmitt and S. Jin, *Science*, 2008, **320**, 1060–1063.
31 A. Indra, P. W. Menezes, N. R. Sahraie, A. Bergmann, C. Das, M. Tallarida, D. Schmeißer, P. Strasser and M. Driess, *J. Am. Chem. Soc.*, 2014, **136**, 17530–17536.
32 C. C. McCrory, S. Jung, J. C. Peters and T. F. Jaramillo, *J. Am. Chem. Soc.*, 2013, **135**, 16977–16987.
33 W. Ma, R. Ma, C. Wang, J. Liang, X. Liu, K. Zhou and T. Sasaki, *ACS Nano*, 2015, **9**, 1977–1984.
34 X. Long, J. Li, S. Xiao, K. Yan, Z. Wang, H. Chen and S. Yang, *Angew. Chem., Int. Ed.*, 2014, **53**, 7584–7588.
35 C. C. L. McCrory, S. Jung, I. M. Ferrer, S. Chatman, J. C. Peters and T. F. Jaramillo, *J. Am. Chem. Soc.*, 2015, **137**, 4347–4357.
36 F. Song and X. Hu, *J. Am. Chem. Soc.*, 2014, **136**, 16481–16484.
37 Y. Surendranath, M. W. Kanan and D. G. Nocera, *J. Am. Chem. Soc.*, 2010, **132**, 16501–16509.
38 S. Gao, Y. Sun, F. Lei, L. Liang, J. Liu, W. Bi, B. Pan and Y. Xie, *Angew. Chem., Int. Ed.*, 2014, **53**, 12789–12793.
39 N. Danilovic, R. Subbaraman, K. C. Chang, S. H. Chang, Y. Kang, J. Snyder, A. P. Paulikas, D. Strmcnik, Y. T. Kim, D. Myers, V. R. Stamenkovic and N. M. Markovic, *Angew. Chem., Int. Ed.*, 2014, **53**, 14016–14021.
40 H. Schmidt, J. C. Rode, D. Smirnov and R. J. Haug, *Nat. Commun.*, 2014, **5**, 5742.